

PAPER • OPEN ACCESS

+Effect of niobium on microstructure and properties of 6016 aluminum alloy

To cite this article: Bo Lu *et al* 2021 *J. Phys.: Conf. Ser.* **2044** 012090

View the [article online](#) for updates and enhancements.

You may also like

- [Rapid bake-hardening response of Al–Mg–Si alloy during two-stage pre-aging heat treatment](#)
Xiaoge Duan, Zhenli Mi, Haitao Jiang et al.
- [Electrochemical and mechanical performance of reduced graphene oxide, conductive hydrogel, and electrodeposited Pt–Ir coated electrodes: an active *in vitro* study](#)
Ashley N Dalrymple, Mario Huynh, Ulises Aregueta Robles et al.
- [Influence of two-stage ageing process and Cu additions on conductive Al alloys based on AA 6063](#)
Shuwei Duan, Kenji Matsuda, Yong Zou et al.

ECS
The
Electrochemical
Society
Advancing solid state &
electrochemical science & technology

DISCOVER
how sustainability
intersects with
electrochemistry & solid
state science research

+Effect of niobium on microstructure and properties of 6016 aluminum alloy

Bo Lu^{1,a}, Anmin Li^{1,2,3,b*}, Chan Wu^{1,c}, Huirong Yang^{1,d}, Yu Rao^{1,e}

¹School of Resources, Environment and Materials, Guangxi University, Nanning, 530004, P.R. China

²MOE Key Laboratory of New Processing Technology for Non-ferrous Metals and Materials, Guangxi Key Laboratory of Processing for Non-ferrous Metals and Featured Materials, Guangxi University, Nanning, Guangxi 530004.

³Center of Ecological Collaborative Innovation for Aluminum Industry in Guangxi, Nanning, 530004, China

^aemail: 1725328722@qq.com,

*corresponding author: ^bemail: lianmin@gxu.edu.cn

^cemail: 1346609235@qq.com, ^demail: 1604424832@qq.com, ^eemail: 2329237760@qq.com

Abstract: 6016 aluminum alloys with different niobium contents were prepared by smelting and casting. The alloys were rolled and heat treated, and the effect of niobium on microstructures and properties of the alloys were studied. The results show that the as-cast alloy consists of Mn-rich phases, Cu-rich phases, Mg-rich phases, Si-rich phases and small blocks of Zn-rich phases, and Nb element is solidly dissolved in these phases and matrix. After solution and pre-aging treatment, recrystallization occurs in the rolled alloy. The grain size of the rolled alloy is obviously smaller than that of the as-cast alloy, and the second phase precipitates dispersively. After solution treatment or solution treatment + pre-aging treatment, the tensile strength and plasticity of the alloy are significantly improved. With the increase of niobium content, the number and size of the second phase increase. The alloy with 1%Nb in T4P condition has the better comprehensive mechanical properties, and its elongation after fracture, tensile strength, yield strength, plastic strain ratio and strain hardening index are as following respectively: 34.20%, 372.77MPa, 208.54MPa, 0.82, 0.32.

1. Introduction

With the development of science and technology, people's ownership and demand for cars is increasing day by day. It has brought serious challenges to the ecological environment. Therefore, the study of automotive lightweight is an important means to achieve energy saving and emission reduction [1-2]. In addition to the advantages of light weight, but also good molding, corrosion resistance and other excellent characteristics, aluminum alloy is widely used in the transportation industry. There is great room for improvement in the rate of automobile aluminum [3].

6016 aluminum alloy is a kind of heat treatment strengthening aluminum alloy. Its application in automobile still has some shortcomings in anti-sag and other aspects. Therefore, it is necessary to



Content from this work may be used under the terms of the [Creative Commons Attribution 3.0 licence](https://creativecommons.org/licenses/by/3.0/). Any further distribution of this work must maintain attribution to the author(s) and the title of the work, journal citation and DOI.

improve its comprehensive properties by microalloying and adjusting the heat treatment process [4]. Studies have shown that adding trace elements such as Sc, Cr and Zr in 6016 aluminum alloy can refine the alloy grain, change the distribution of the second phase, promote its dispersion and uniform precipitation, and improve the properties of the alloy [5-7]. Xiaowu Hu et al. [8] found that, in ADC12 aluminum alloy added rare earth Er, the distance between the secondary dendritic arms was shortened, and the rough flak-like and acicular eutectic silicon was transformed into fibrous and slender branches, and the tensile strength of the alloy was improved. Q. Zhao et al. [9] found that adding Zr and Er to 6 series aluminum alloys could shorten the aging time and improve the aging strengthening effect. Liu Quan et al. [10] found that the addition of Nb to aluminum alloy can refine the Mn-rich phase, and promote the formation of $Al_{15}Mn_3Si_2$ needle equivalent, and improve the mechanical properties of the alloy at 300°C~350°C.

At present, there are few studies on Nb alloying 6016 aluminum alloy. In this paper, the effects of adding different Nb content on the microstructure and mechanical properties of 6016 aluminum alloy under different processing states were investigated. The experimental results will provide reference for the actual production of 6016 aluminum alloy.

2. Experiment Procedure

The composition design of 6016 aluminum alloy is shown in Table 1. The raw materials are pure aluminum (99.9%), Al-20Si, Al-50Cu, Al-10Mn, Al-10Mg, Al-20Cr, Al-20Zn, Al-50Nb, etc. According to the preset experimental alloy composition, five groups samples with different Nb content were melted by melting furnace at 750°C and casted in a steel mold at 300°C. The as-cast alloy was homogenized at 550°C for 10 hours and then rolled to obtain a plate of 1mm thickness. The samples were cut and subjected to heat treatment: 550°C×10min, water quenched at room temperature. Some of them were naturally aged to form T4 samples, while the others were pre-aged (170°C×10min) and were naturally aged to form T4P samples.

Table 1 Composition of 6016 aluminum alloy (mass fraction, %)

Samples	Si	Cu	Mn	Mg	Cr	Zn	Ti	Nb	Al
0#	1.10	0.40	0.13	0.47	0.03	0.20	0.02	0	Balance
1#	1.10	0.40	0.13	0.47	0.03	0.20	0.02	0.25	Balance
2#	1.10	0.40	0.13	0.47	0.03	0.20	0.02	0.50	Balance
3#	1.10	0.40	0.13	0.47	0.03	0.20	0.02	0.75	Balance
4#	1.10	0.40	0.13	0.47	0.03	0.20	0.02	1.00	Balance

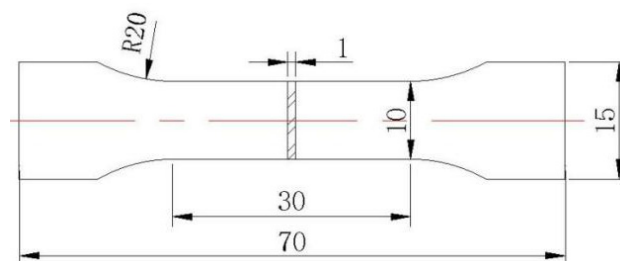


Fig.1 Size diagram of tensile specimen

The metallographic specimens were treated with 5%HF. The microstructures were analyzed by polarized light microscopy (OM; DM2500) and field emission scanning electron microscopy (SEM; SU8020). Image-Pro Plus 6.0(IPP) Image software was used for data processing and measurement. Multiple parallel samples of each type of as-cast sample were taken for grain statistics, and at least 200 grains of each type of heat-treated sample were taken for grain statistics to get the average grain size. Hardness test was performed using a nano-micro indentation (NVM-100) durometer with a load of 0.1kg for 15 seconds. Multiple positions of each sample were measured and their average values were taken. Meanwhile, according to GB/T 228.1-2010, 6016 aluminum alloy under different heat treatment

state was processed into national standard tensile samples paralleling to the rolling direction (0°), and the size of the tensile samples was shown in Fig.1. The stretching machine was the British Universal Testing Machine (8801), and the tensile test was carried out at a speed of 2mm/min. Three standard samples of each test were measured with a vernier caliper to calculate the elongation and take the average value. In addition, the tensile fracture was analyzed by scanning electron microscopy (SEM).

3. Results and Discussion

3.1 Microstructures analysis

Fig. 2 shows the microstructures of as-cast 6016 aluminum alloy. It shows that there are a few holes, the grain size is not uniform, the precipitated phase is mostly distributed in the grain and dispersed (the black particles in Fig. 2). Fig. 2 (f) is the average grain size. It can be seen that the grain size of the alloy with Nb is less than that of the 0# sample. When the niobium content increases from 0% to 0.75%, the grain refinement effect becomes more and more obvious, the grain shape is more regular and the grain size is more uniform. In the process of casting and solidification, due to the limitation of diffusion, Nb element is easy to segregate in solidification front, which leads to the subcooling of the structure, reduces the eutectic temperature, and hinders the transformation of the alloy from the liquid phase to the solid phase. Some researchers think that grain refinement effect results from the metal compounds containing more rare earth Nb disperse in the grain boundary which slows down the growth rate of the α -Al grain [11-12]. When Nb content (1%) increases, the grain size of 4# sample increases, and some small grains appear, which increases the inhomogeneity of grain size. However, the number of precipitates increases and they are located closer to the grain boundary (as shown in Fig. 2(e) at the black circle).

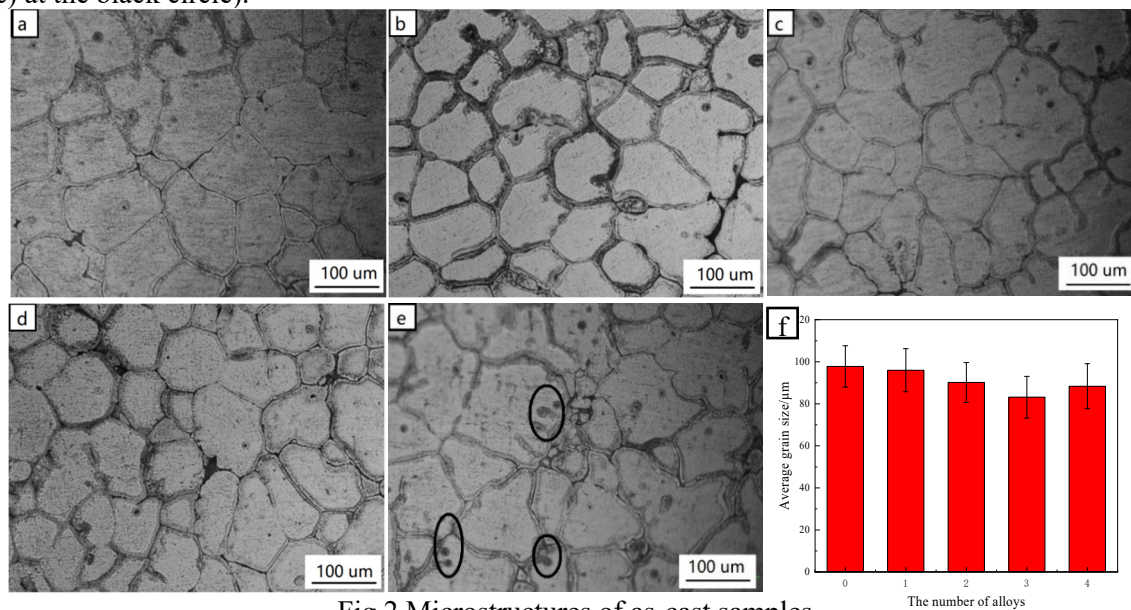


Fig.2 Microstructures of as-cast samples

(a) 0# ; (b) 1# ; (c) 2# ; (d) 3# ; (e) 4# ; (f) Average grain size of samples

Fig. 3 shows the microstructures of the T4P samples. After rolling, the microstructure of the alloy is flat and fibrous. After solution treatment and pre-aging treatment, recrystallization occurs. As can be seen from Fig.2 and Fig.3, the grain size of T4P sample is obviously smaller than that of as-cast alloy; this result of fine-grain strengthening is consistent with that of increasing the plasticity of T4 and T4P samples in the following tensile test.

As shown in Fig. 3(a)-(b), there are large precipitates in the alloy, and they are concentrated at the grain boundary and have a pinning effect on the grain boundary, which inhibits the grain growth. Therefore, the grain size of 0# and 1# sample is small. It can be seen clearly from Fig. 3(c), (d) and (e) that the number and size of the dispersed phase in the T4P samples increase with the increase of Nb.

The grain size of 4# sample is slightly smaller than that of 3# sample. This may result from the more and larger size of precipitates in 4# sample, which nails the grain boundary and inhibits the grain growth. The second phase strengthening and fine grain strengthening are significant, which correspond to the results of the highest yield strength and tensile strength of T4P samples.

Fig. 4 shows the microstructures of the as-cast samples. Table 2 shows the results of energy spectrum analysis for each region in Fig. 4. It can be seen that the alloy has a massive white-gray Mn-rich phase (such as Fig.4 area A), an elliptical strip-like Cu-rich phase (area B), an irregular and small magnesium-rich phase (area C) near the grain boundary, a discontinuous band-like Si-rich structure (area D) and a small massive Zn-rich phase (area E). Nb is dissolved in these phases. However, these rare earth phases have higher melting points and hardness, which can be used as strengthening phases to improve the mechanical properties of materials [13-14].

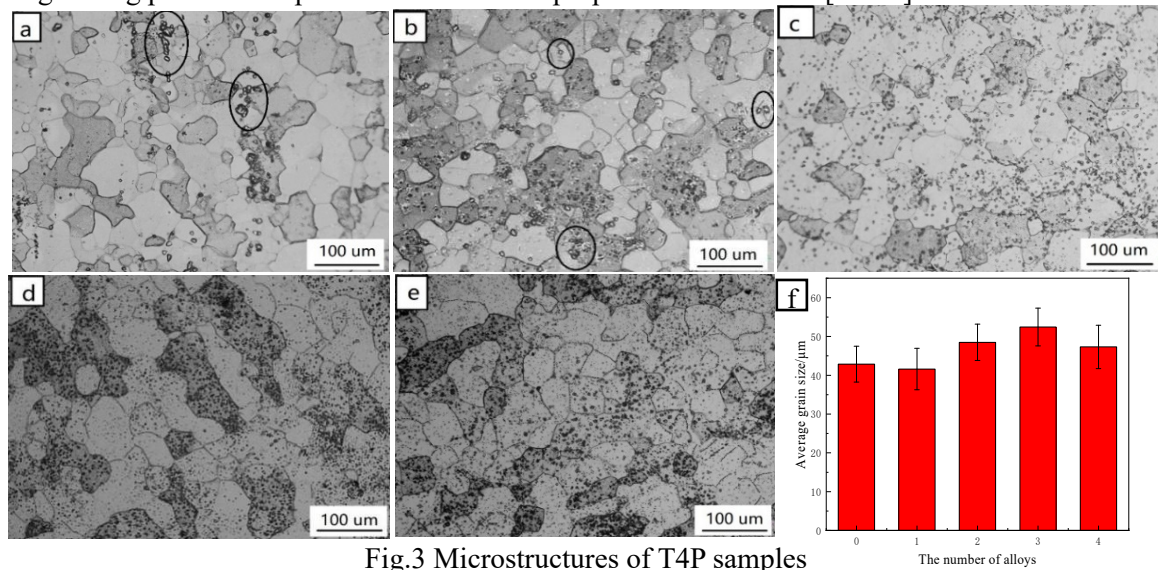


Fig.3 Microstructures of T4P samples
 (a) 0# ; (b) 1# ; (c) 2# ; (d) 3# ; (e) 4# ; (f) Average grain size of samples

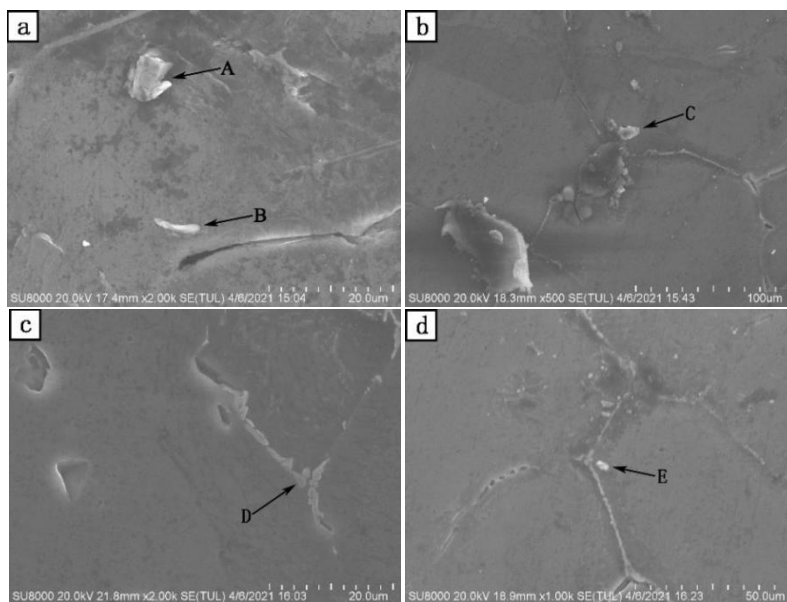


Fig.4 SEM analysis of as-cast samples
 (a) 0# ; (b) 1# ; (c) 2# ; (d) 3# ; (e) 4# ;

Table 2 Results of energy spectrum analysis of characteristic points of each sample (mass fraction, %)

Area	Al	Si	Cu	Mn	Mg	Mn	Cr	Fe	Nb	Ni
A	76.08	0.55	-	22.30	0.26	-	-	0.51	-	-
B	97.77	-	1.14	0.16	0.66	-	-	0.18	-	-
C	98.17	-	-	-	0.93	0.08	-	-	0.82	-
D	54.93	41.26	1.53	0.42	1.41	-	-	-	0.45	-
E	66.11	10.03	0.31	-	1.34	0.18	20.76	0.41	0.47	0.40

3.2 Hardness analysis

The hardness values of the as-cast and T4P samples were tested as shown in Fig. 5. It is found that the hardness of T4P sample is much higher than that of the as-cast sample. With the increase of Nb content, the hardness of T4P samples decreases.

As shown in Fig.5, the trend of hardness change of the as-cast samples is basically the same as that of the T4P samples, and the trend is : increase→decrease→increase. The hardness value (85.76HV) of the 4# as-cast sample (1%Nb) is the highest. The reason may be that the microstructures of small grains are distributed in the large grains as the front analyse. There is another reason: as the alloying elements dissolve in the matrix, the lattice distortion of the matrix is intensified, and the dislocation movement is hindered, so that the alloy is strengthened and the hardness is increased [15].

Compared to the corresponding as-cast sample, the hardness improvement value (23.71HV) of the 4# T4P sample is less than the others. It may be because the alloy elements precipitate out as the second phase after solution and pre-aging treatment. For example, according to the metallographic structure of 4# sample in Fig. 3 (e), it can be seen that the second phase precipitated is larger in size and quantity, and the lattice distortion of the matrix is relieved. It is speculated that the strengthening effect of the second phases in this alloy is weaker, which makes the hardness increase less. The hardness improvement value (52.45HV) of 1# T4P sample is larger, which is 68.5% higher than that of the as-cast .

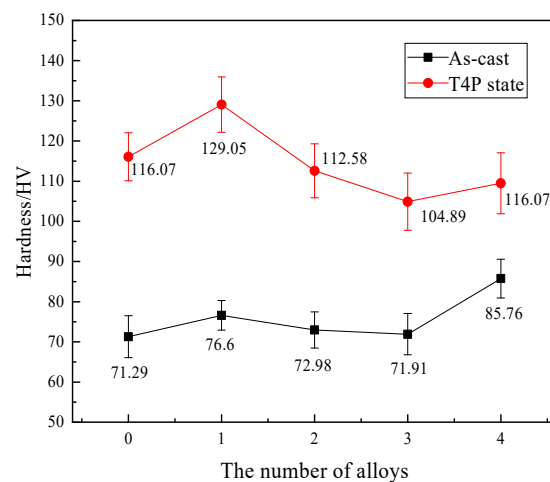


Fig.5 Hardness values of each group of samples

3.3 Tensile property analysis

Tensile tests were carried out at room temperature for the rolled, T4 and T4P samples. The strain-hardening index n reflects the ability of the material to resist plastic deformation, and represents the ability of the material to make uniform deformation by hardening before the necking occurs. It is a

performance index to characterize the strain-hardening behavior of metal materials. The strain hardening index n is a function of true stress and true strain as formula (1) [16]. Taking the logarithms of both sides of equation (1) and drawing a straight line diagram, the slope of this line is the strain hardening exponent. The calculation formula of true stress S is shown as formula (2), and the calculation of true strain e is shown as formula (3).

$$S = Ke^n \tag{1}$$

$$S = F/A = F/(A_0 \times l_0/(l_0 + \varepsilon)) \tag{2}$$

$$e = \varepsilon/(l_0 + \varepsilon) \tag{3}$$

The plastic strain ratio r is the ratio of the true strain in the width direction and the true strain in the thickness direction in the specimen gauge distance when the specimen is uniaxially stretched to produce the uniform plastic deformation. It is the most important parameter to evaluate the deep drawing property of metal sheet. It reflects the ability of a metal sheet to resist thinning or thickening when the material is subjected to tension or pressure. The plastic strain ratio can be calculated according to formulas (4), (5) and (6).

$$r = \varepsilon b/\varepsilon a \tag{4}$$

$$\varepsilon b = \ln(b_1/b_0) \tag{5}$$

$$\varepsilon a = \ln(a_1/a_0) \tag{6}$$

b_0 and a_0 are the original width and thickness of the specimen, b_1 and a_1 are the dimensions of the specimen after drawing.

Fig.6 shows the tensile stress-strain curves of 6016 aluminum alloy samples. Table 3 shows the results of tensile test, work hardening coefficient (n) and plastic strain ratio (r) of the samples.

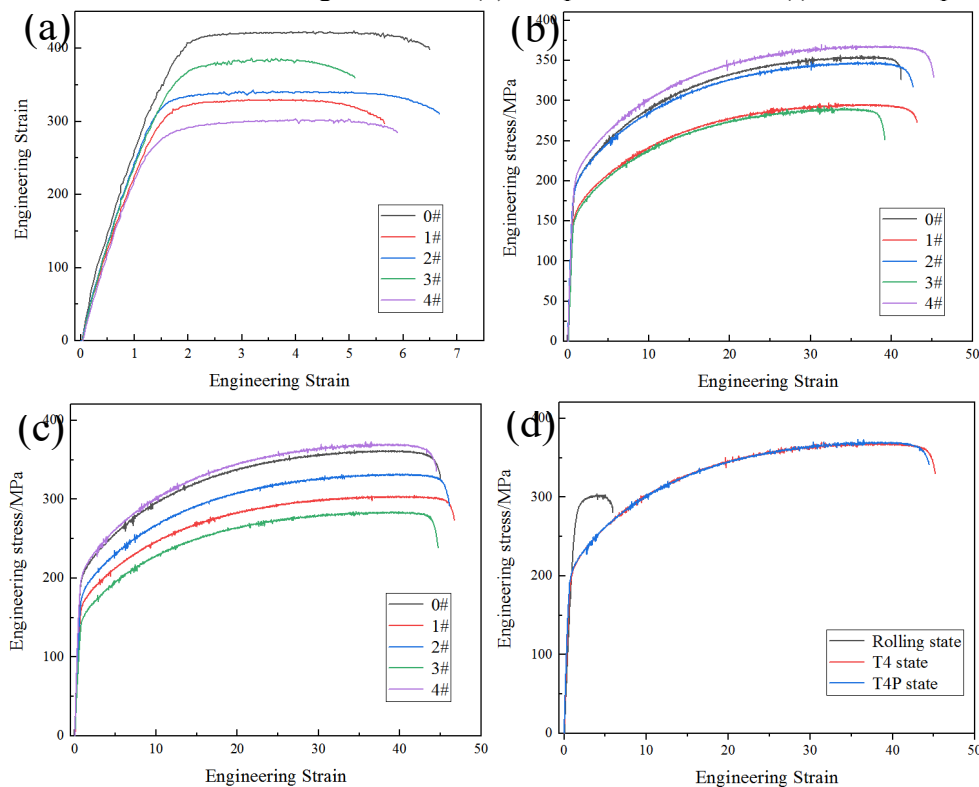


Fig.6 Tensile stress-strain curves of 6016 aluminum alloy samples

(a) Rolled; (b) T4; (c) T4P; (d) Comparison of tensile curves of rolled, T4 and T4P 4# samples

From Fig.6 and Table3, the highest yield strength, tensile strength and ductility of the rolled samples are 258.90 MPa (3# sample), 424.01 MPa (0# sample) and 6.84% (2# sample) respectively. For all T4 samples, the yield strength, tensile strength and elongation of 4# T4 sample are the highest, and the comprehensive mechanical properties are better. In addition, with the increase of Nb content, the plastic strain ratio of the alloys tends to decrease. But the 4# sample has the highest strain

hardening index (0.35), which indicates that it has high resistance to continuous plastic deformation and is not easy to produce necking and fracture [17]. For the T4P samples, first, n decreases, then increases with the increase of Nb content. The n values of the 0# and 4# samples is the highest, but the yield strength (208.54 MPa) and tensile strength (372.77 MPa) of 4# sample are the highest. The r value of the 1# sample is the highest, which shows that its uniform deformation ability and plasticity are better, and its elongation after breaking can reach 35.12%.

The plastic strain ratio and elongation after fracture of 1# sample are slightly higher than that of 4# sample, but the yield strength and tensile strength of the 4# sample are obviously higher than that of the 1# sample. Considering the comprehensive strength and plasticity, the comprehensive properties of 4# sample are better.

As can be seen from Fig.6 (d), after solution treatment or solution treatment + pre-aging treatment, the tensile strength and plasticity of the alloy increase significantly. The tensile strength values of T4 and T4P samples obviously increase resulting from fine grains after recrystallization and precipitation of dispersion strengthened phase after aging because grain boundary and the second phases hinder dislocation movement. In addition, the smaller the grain size is, and the more the dislocation slip sites is, the higher the dislocation slip ability is and the higher the alloy plasticity is.

Table 3 Mechanical property of the samples

Samples		Yield strength (MPa)	Tensile strength (MPa)	Elongation (%)	Work hardening coefficient (n)	Plastic strain ratio (r)
rolled	0#	216.41	424.01	6.80	0.51	0.68
	1#	206.09	330.01	5.88	0.43	0.76
	2#	232.79	343.15	6.84	0.45	0.77
	3#	258.90	386.43	5.58	0.48	0.73
	4#	237.01	303.88	6.72	0.46	0.74
T4	0#	193.51	357.22	31.24	0.34	0.72
	1#	156.04	297.54	31.04	0.32	0.73
	2#	190.79	348.59	32.36	0.33	0.80
	3#	154.51	292.95	29.80	0.30	0.76
	4#	208.77	369.71	33.68	0.35	0.68
T4P	0#	202.37	362.11	33.60	0.32	0.69
	1#	169.13	304.72	35.12	0.31	0.75
	2#	187.01	331.98	34.08	0.30	0.69
	3#	149.07	284.23	33.64	0.29	0.61
	4#	208.54	372.77	34.20	0.32	0.73

Fig.7 shows the tensile fractures of the T4P samples. A large number of dimples can be seen in Fig.7, which helps to judge that the tensile fracture of T4P sample belongs to ductile fracture. 1# sample has smaller dimples, more dimples and deeper dimples. 4# sample has larger dimples and fewer dimples, and most dimples are shallow. The size of the dimple determines the degree of ductile fracture. The more uniform and deeper the dimples are, the better the ductility of the alloy is [18]. For samples with small dimples, the microcracks selectively expand after loading until the crack source is generated. When the crack expands to the grain boundary, the grain boundary will prevent the crack

growth [19]. Therefore, the ductility of 1# sample is slightly higher, and the elongation at break is higher. In general, the results of fracture morphology are consistent with the change of fracture mode and ductility of different specimens.

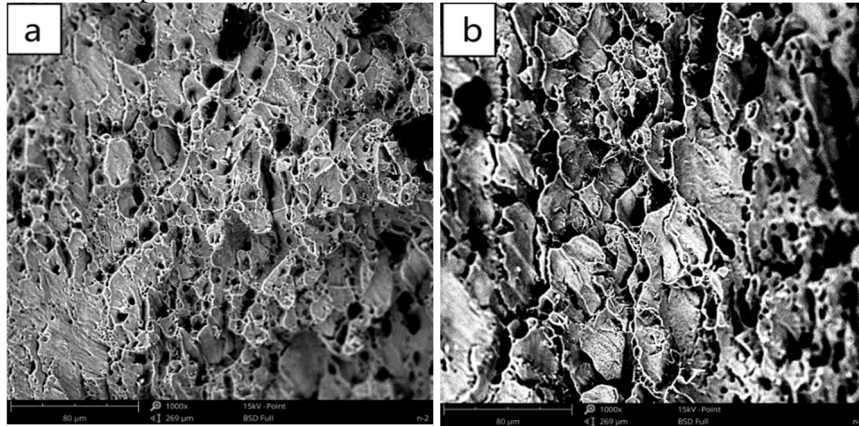


Fig.7 Tensile fractures of T4P samples at room temperature

(a) 1#; (b) 4#

4. Conclusion

6016 aluminum alloys with different Nb content were prepared by melting, rolling and solution treatment to obtain the rolled, T4, T4P samples. The microstructures and mechanical properties of rolled, T4 and T4P samples were analyzed, and the conclusion is as the following :

(1) there are massive white-gray Mn-rich phases, elliptical strip-like Cu-rich phases, irregular small massive Mg-rich phases near grain boundaries, discontinuous strip-like Si-rich structures at grain boundaries and small massive Zn-rich phases in as-cast alloys, Nb is dissolved in these phases and in the Matrix.

(2) T4P samples underwent solution, pre-aging treatment, recrystallization, grain size refinement, and the second phase dispersion precipitation. With the increase of Nb content, the number and size of the dispersion phase increase.

(3) The trend of hardness change of the T4P samples is consistent with that of the as-cast samples. With the increase of Nb content, the hardness increases first, then decreases and last increases.

(4) After solution treatment or solution treatment + pre-aging treatment, the tensile strength and plasticity of the alloy are significantly improved. The alloy with 1%Nb in T4P condition has the better comprehensive mechanical properties, and its elongation after fracture, tensile strength, yield strength, plastic strain ratio and strain hardening index are as following respectively: 34.20%, 372.77MPa, 208.54MPa, 0.82, 0.32.

Acknowledgement

This study was funded by found project of the Project Sponsored by MOE Key Laboratory of New Processing Technology for Non-ferrous Metals and Materials, Guangxi Key Laboratory of Processing for Non-ferrous Metals and Featured Materials (2021GXMPSTF02), and The First Batch of Guangxi Innovation-driven Development Projects in 2017 (Major Project of Science and Technology) (Guike AA17202008).

References

- [1] Zhou J, Wan X, Li Y. Advanced Aluminium Products and Manufacturing Technologies Applied on Vehicles Presented at the EuroCarBody Conference. *Materials Today: Proceedings*, 2015, 2(10): 5015-5022.
- [2] Henriksson, F. and K. Johansen, On Material Substitution in Auto-motive BIWs – From Steel to Aluminum Body Sides. *Procedia CIRP*, 2016. 50:683-688.
- [3] Xu, C., et al., The synergic effects of Sc and Zr on the microstructure and mechanical properties of

- Al–Si–Mg alloy. *Materials & Design*, 2015. 88:485-492.
- [4] Li Hui, Zhang Hua, Zhu Zhenfeng, et al. Influence of pre-aging time on microstructure and mechanical properties of 6016 aluminum alloy for automobile[J]. *Heat Treatment of Metals*, 2016,41(12):149-152
- [5] Xu, C., et al., The synergic effects of Sc and Zr on the microstructure and mechanical properties of Al–Si–Mg alloy. *Materials & Design*, 2015. 88:485-492.
- [6] Santos, A., S. Costa, and A.M. Pinto, Effect of Sc Additions on the Modification of Eutectic Si of As Cast Al-9wt%Si Alloy. *Microsc Microanal*, 2015. 21 Suppl 5:43-4.
- [7] Xinming Zhang, Xingxing Liu, Jianguo Tang, et. al. Effect of joint added Mn, Cr and Sr on microstructure and mechanical properties of 6016 alloy used for automotive body sheets[J]. *Journal of Central South University (Science and Technology)*, 2014, 45(12): 4152-4160.
- [8] Xiaowu Hu, Fugang Jiang, Fanrong Ai, et. al. Effects of rare earth Er additions on microstructure development and mechanical properties of die-cast ADC12 aluminum alloy[J]. *Journal of Alloys and Compounds*, 2012, 538.
- [9] Q. Zhao, H.J. Huang, X.G. Yuan, F.Y. Dong, P. Zhao, Aging pre-cipitation and strengthening behavior of Al-Mg-Si alloy sheets con-taining Er and Zr element, *J. Mater. Heat Treat.* 2015, 36(11): 40-46 (in Chinese).
- [10] Qu Liu. Alloying and micro alloying on novel heat-resistant alloy used for automobile engine block[D]. Southeast University, 2017: 84-92.
- [11] Dong, Y., et al., Investigation on the modification behavior of A356 alloy inoculated with a Sr-Y composite modifier. *Journal of Rare Earths*, 2013. 31(2):204-208.
- [12] X.M. Cheng, J.Q. Han, Y.G. M, et al., Effect of Ce on microstructure and properties of 6063 aluminum alloy for electric purpose,J. *Hot Working Technology*. 2018, 47(20): 38-41
- [13] S.F. Liu, et al., Effect of Yttrium Addition on As-cast Microstructure and Properties of 6063 Aluminum Conductors. *Journal of the Chinese Society of Rare Earths*, 2018,36(2):202-207.
- [14] Wei, Z., et al., Microstructure and mechanical properties of A356 alloy with yttrium addition processed by hot extrusion. *Journal of Rare Earths*, 2019. 37(6):659-667.
- [15] Ding, W., et al., Effect of rare earth Y and Al–Ti–B master alloy on the microstructure and mechanical properties of 6063 aluminum alloy. *Journal of Alloys and Compounds*, 2020. 830.
- [16] Wei, Z., et al., Microstructure and mechanical properties of A356 alloy with yttrium addition processed by hot extrusion. *Journal of Rare Earths*, 2019. 37(6):659-667.
- [17]Xiaoxue An, Study on Heat Treatment of 6016 Aluminum Alloy Sheets for Automotive Body[D]. Northeastern University, 2014:16-18.
- [18] Singh RK, Singh AK, Prasad NE. Texture and mechanical property anisotropy in an Al–Mg–Si–Cu alloy. *Mater. Sci. Eng., A* 2000;277:114–22.
- [19] P. Dai, X. Luo, Y.Q. Yang, Z.D. Kou, B. Huang, C. Wang, J.X. Zang, J.G. Ru, Nanoscale precipitate evolution and mechanical properties of 7085 aluminum alloy during thermal exposure, *Mater. Sci. Eng., A* (2018) 411-422.